Lattice-Boltzmann Simulations of Multiphase Flows in Gas-Diffusion-Layer (GDL) of a PEM Fuel Cell

Shiladitya Mukherjee[a], J. Vernon Cole[a], Kunal Jain[b], and Ashok Gidwani[a]

[a] CFD Research Corporation, Huntsville, Alabama 35805, USA
[b] ESI US R&D Inc, Huntsville, Alabama 35806, USA

Introduction

Improved power density and freeze-thaw durability in automotive applications of Proton Exchange Membrane Fuel Cells (PEMFCs) requires effective water management at the membrane. This is controlled by a porous hydrophobic gas-diffusion-layer (GDL) inserted between the membrane catalyst layer and the gas reactant channels. The GDL distributes the incoming gaseous reactants on the catalyst surface and removes excess water by capillary action. There is, however, limited understanding of the multiphase, multi-component transport of liquid water, vapor and gaseous reactants within these porous materials. This is due primarily to the challenges of in-situ diagnostics for such thin (200 – 300 μ), optically opaque (graphite) materials. Transport is typically analyzed by fitting Darcy's Law type expressions for permeability, in conjunction with capillary pressure relations based on formulations derived for media such as soils. Therefore, there is significant interest in developing predictive models for transport in GDLs and related porous media. Such models could be applied to analyze and optimize systems based on the interactions between cell design, materials, and operating conditions, and could also be applied to evaluating material design concepts.

Recently, the Lattice Boltzmann Method (LBM) has emerged as an effective tool in modeling multiphase flows in general [1-3], and flows through porous media in particular [4-6]. This method is based on the solution of a discrete form of the well-known Boltzmann Transport Equation (BTE) for molecular distribution, tailored to recover the continuum Navier-Stokes flow [7,8]. The kinetic theory basis of the method allows simple implementation of molecular forces responsible for liquid-gas phase separation and capillary effects. The solution advances by a streaming and collision type algorithm that makes it suitable to implement for domains with complex boundaries. We have developed both single and multiphase LB models and applied them to simulate flow through porous GDL materials. We will present an overview of the methods as implemented, verification studies for both microstructure reconstruction and transport simulations, and application to single- and two-phase transport in GDL structures. The applications studies are designed to both improve understanding of transport within a given structure, and to investigate possible routes for improving material properties through microstructure design.

Numerical Model

In this section, we describe implementation of a multi-dimensional, multi-phase Lattice-Boltzmann Model (LBM) with a model for surface wettability, and the reconstruction scheme for the porous gas-diffusion-layer (GDL).

The Lattice-Boltzmann Model (LBM)

The LBM is based on well-known Boltzmann Transport Equation (BTE) given by,

$$\frac{Df(\mathbf{x},\boldsymbol{\xi},t)}{Dt} = \frac{\partial f}{\partial t} + \boldsymbol{\xi}.\nabla f + \mathbf{F}.\nabla_{\xi} f = \left(\frac{\partial f}{\partial t}\right)_{coll} \quad [1]$$

Here, f is the probability distribution function describing distribution of particle population over velocities $\boldsymbol{\xi}$, at location $\mathbf{x}$ at time t and $\mathbf{F}$ is the mean-molecular interaction force. The right side of the equation is the rate of change in f due to intermolecular collisions. f is related to the local density ρ and momentum $\rho\mathbf{u}$ as,

$$\rho(\mathbf{x},t) = \int f(\mathbf{x},\boldsymbol{\xi},t)d\boldsymbol{\xi} \quad [2]$$

$$\rho(\mathbf{x},t)\mathbf{u}(\mathbf{x},t) = \int f(\mathbf{x},\boldsymbol{\xi},t)\boldsymbol{\xi}d\boldsymbol{\xi} \quad [3]$$

In LBM, the collision operator is modeled by Bhatanagar-Gross-Krook (BGK) model [9],

$$\left(\frac{\partial f}{\partial t}\right)_{coll} = -\frac{f - f^{eq}}{\lambda} \quad [4]$$

The Boltzmann model assumes that particle distributions approach local equilibrium linearly over a characteristic time λ. This characteristic time is related to fluid viscosity ν. While simple, this model has well-known limitations in applications such as multiphase and porous media flow. In particular, for porous media flow, employing the BGK model results in viscosity dependence of the computed permeability. We have also reconfirmed this observation through our own set of simulations. Hence, in this work, a multiple-relaxation-time (MRT) collision model is implemented [8,10]. In the MRT model, the single relaxation time λ is replaced by a collision-matrix given by,

$$\left(\frac{\partial f_{\alpha}}{\partial t}\right)_{coll} = -\Lambda_{\alpha\beta}(f_{\beta} - f_{\beta}^{eq}) \quad [5]$$

Here, α, β corresponds to particle velocities $\boldsymbol{\xi}_{\alpha}$ and $\boldsymbol{\xi}_{\beta}$, respectively. Employing the collision-matrix allows separation of relaxation time-scales between hydrodynamic modes such as velocity, pressure and stress-tensors, thus improving numerical accuracy and stability.

Multiphase LBM

In the multiphase model of He et al. [1], the mean-molecular interaction force $\mathbf{F}$ is formulated as sum of a phase segregation and surface tension force. The phase segregation force is expressed as the gradient of the non-ideal part of the equation-of-states (EOS), which separates the fluid into respective liquid and gas phase densities by entropy minimization. The surface tension force depends on the interfacial curvature, and is scaled by the strength of the molecular interaction.

In numerical implementation, two separate distribution functions are used. One distribution function f is for a phase-tracking variable, known as the index-function φ. The transport equation of f

recovers an advection-diffusion equation known as the Cahn-Hilliard equation. Transition of φ from the limiting values at the liquid to gas phase occurs over finite number of lattice nodes. The interface is implicitly defined as the contour of φ having the average of these limiting values. Fluid properties, such as, density and viscosity are interpolated from φ. A second distribution function g is used to compute pressure and momentum. The transport equation of g recovers the Navier-stokes equation with a surface tension term. The surface tension is computed from φ as proportional to $\varphi\nabla\nabla^2\varphi$. In this work, the first and second-order derivatives are computed as weighted sum of the second-order central difference along the lattice-velocity directions. The limiting values of φ are obtained analytically from the EOS and can be further refined from the simulation of liquid film or drop equilibration.

Surface Wettability

Mukherjee et al. [2] modeled wettability by adding an external force near the surface, mimicking molecular attraction/repulsion between liquid drop molecules and solid surface molecules as,

$$\mathbf{F}_w = -K_w \varphi_l \mathbf{n}_s \qquad [6]$$

Here, K_w is the strength of interaction parameter and $\mathbf{n}_s$ is the surface normal. In this work, we employ a similar model by Yiotis et al. [11] for its simplicity in implementing on complex boundaries, such as, randomly oriented fibers. The model assigns a φ value to the solid, between the liquid and gas limits to compute surface tension forces near the solid boundary.

Microstructure Reconstruction

The fiber morphology of Toray and SGL non-woven carbon papers are generated as continuous cylinders of fixed diameter f_d, with their axis along parallel planes separated by a spacing of f_d. Within a plane the fibers are randomly orientated and may intersect each other. This approach is similar to that reported by Schulz et al. [4].

Results and Discussions

Single-phase Gas Permeability

The single phase LB model is benchmarked against the test cases of decaying Taylor Vortices and pressure-driven channel flow. The model is then used to simulate gas flow through numerically reconstructed porous material and compute absolute permeability. Figure 1 shows an idealized porous structure of simple-cubic (SC) arrangement of solid spheres. The permeability is computed from the average flow velocity u by applying Darcy's law,

$$u = \frac{\kappa}{\mu\varepsilon}\left(\frac{P_{in} - P_{out}}{L}\right) \qquad [7]$$

Here, κ is the permeability, ε the porosity, μ the viscosity, P the pressure, and L the channel length. In Table 1, computed permeability is compared with the analytical solution of Chapman and Higdon [12] at different porosity by varying the sphere size. The values are in agreement within 5% of the analytical solution.

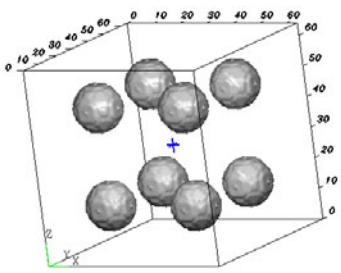

(a) Solid spheres

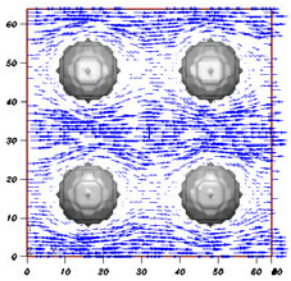

(b) Flow around spheres

TABLE 1. Non-Dimensional Permeability of Simple-Cubic (SC) Arrangement of Spheres.

Porosity, ε	Analytical, κ/d^2	Computed, κ/d^2	% Error
0.992	0.2805	0.2843	1.3
0.935	0.0761	0.0749	1.6
0.779	0.0192	0.0189	1.6
0.477	0.0025	0.0026	4

Figure 1. Flow through simple-cubic arrangement of solid spheres.

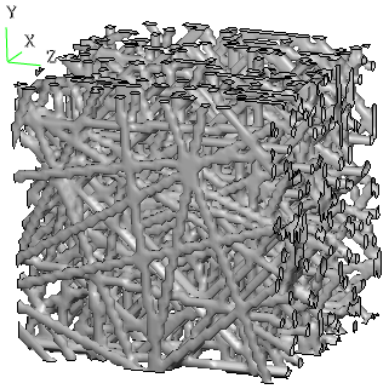

Carbon paper

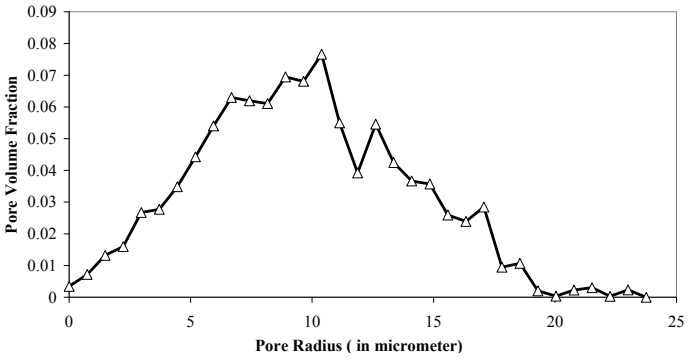

Pore size distribution

Figure 2. Numerically reconstructed carbon paper and its pore size distribution. The porosity is 0.78, comparable to commercially available Toray090.

TABLE 2. Carbon-Paper Microstructure Permeability.

Material	Measured	Simulation	% Error
Toray090 (Through-plane)	8.3	6.241	-24.8
Toray090 (In-plane)	-	8.647	-
SGL10BA (Through-plane)	18	21.71	20.6
SGL10BA (In-plane)	33	30	9.1

Next, in-plane and through-plane permeability are computed for Toray090 and SGL10BA with porosity 0.78 and 0.88, respectively. In Figure 2 numerically generated microstructure for Toray090 is shown. The reconstructed GDL is 200μm thick with spatial resolution of 3.4μm. In Table 2, the computed and measured values of κ are compared. The values are in the unit of *darcy* (10^{-12} m^2). SGL10BA has higher permeability than Toray090 due to higher porosity. The in-plane permeability is greater than through-plane value. The difference is due to the preferred fiber orientation in the material plane and suggests that alignment to the mean-flow direction have less resistance to the flow. The

computed trends are consistent with these observations and are similar to those reported in the numerical work of Schulz et al. [4].

Influence of fiber orientation on permeability is investigated next. Figure 3 shows microstructures when the fibers are constrained to orient within an angle of φ with the y-axes in the in-plane. Permeability is plotted in Figure 6. The κ_{th} decreases with decreasing φ, however, the change is rather small. As example, κ_{th} at $\varphi = 5°$ and 90° are within 15%. The effect is more pronounced in the in-plane direction. Here, $\kappa_{in,z}$ increases by about 75% and $\kappa_{in,y}$ decreases by 47% as φ is lowered from 90° to 5°. The results suggest that the in-plane permeability can be increased significantly along a preferred direction by orienting the fibers along it, without resulting in significant drop of through-plane permeability. This information can be used to enhance gas-diffusion in GDL. The GDL-material can be constructed in two layers. The gas-channel side consisting of fibers with preferred orientations, assisting in-plane gas flow between neighboring gas-channels, and the catalyst side having fibers randomly oriented thereby allowing uniform distribution of incoming gas on the reaction sites.

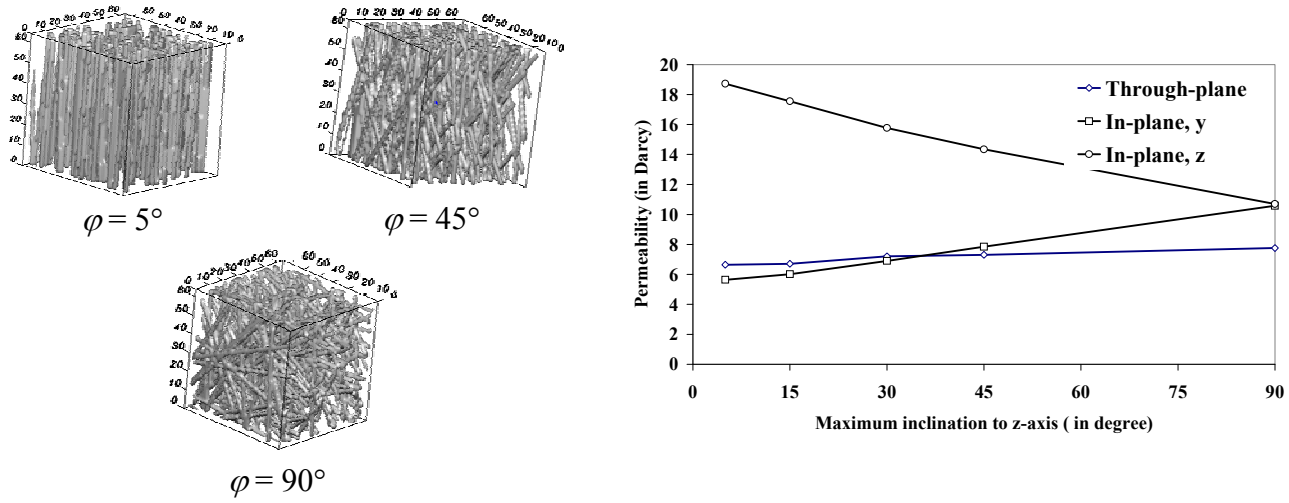

Figure 3. Through and In – plane permeability at various fiber-orientations.

Porous microstructure under external compression is modeled following the same approach as by Schulz et al. [4] i.e. by linearly scaling the height of the solid voxels from the base of the material. Figure 4 shows Toray090 microstructure at $c = 0.6$ and 0.8 and through-plane gas-permeability at different compression ratios for Toray090 and SGL10BA. The measured data is by Dohle et al. [13] on SGL10BA. At higher compression, the GDL thickness decreases but there is no change in the fiber volume. Therefore, porosity and permeability decreases. Computed and measured data are consistent with this expectation.

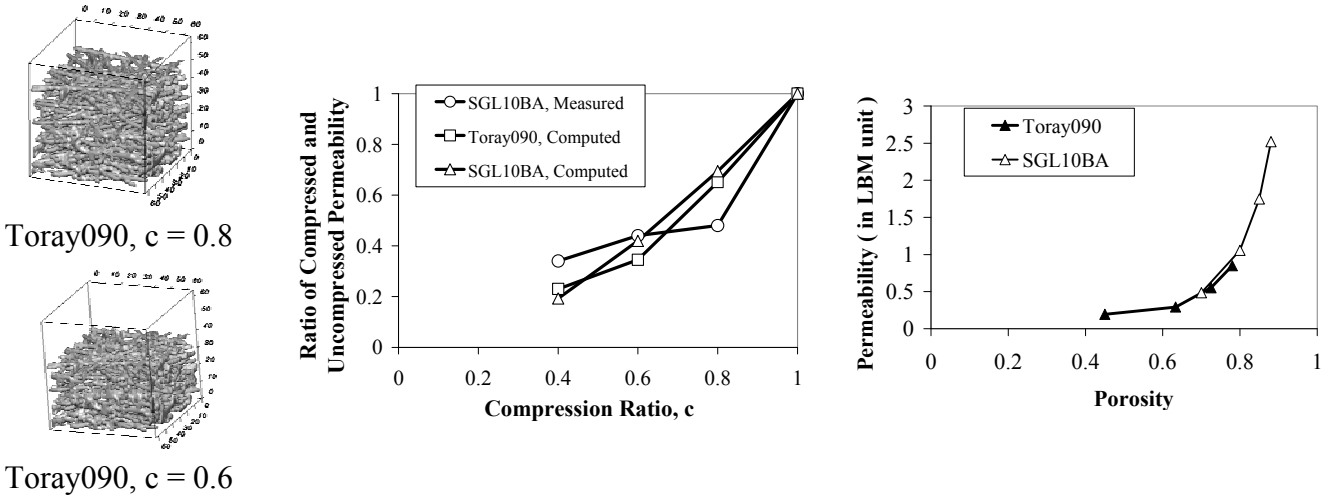

Figure 4. Permeability of Toray090 and SGL10BA under compression.

Multiphase Transport - Capillary Effect

The surface wettability model is validated by simulating drop equilibration on a partially wetted surface. Initially the drop is set to a hemispherical shape corresponding to the contact angle of 90°. As it equilibrates the contact angle may differ depending on the wetting/non-wetting property of the surface. In Figure 5 shape of the equilibrium drop is shown at various wettability including hydrophilic, hydrophobic and neutral.

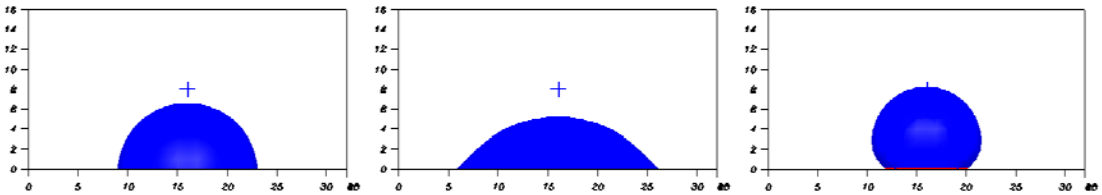

(a) Neutral (b) Hydrophilic (c) Hydrophobic

Figure 5. Drop in equilibrium on partially wetting surfaces.

Figure 6 shows liquid drainage and imbibitions due to capillary action. Initially a tube with circular cross-section is half filled with liquid. The inlet and outlet pressures are set as equal. As the wetting property of the tube is set to hydrophobic, neutral or hydrophilic the liquid-gas interface moves due to capillary pressure. The liquid drains out of the tube when θ_{eq}>90°, fills in the tube when θ_{eq}<90°, and remains stationary when θ_{eq}=90°.

Parallel flow of liquid and gas in a channel is shown in Figure 7. The flow is driven by an imposed pressure gradient between inlet and outlet. The liquid to gas density and viscosity ratios are set to 10. As the flow evolves the liquid-gas interface stays parallel to the flow direction, however, velocity in the gas is greater than the liquid velocity due to lower density and viscosity.

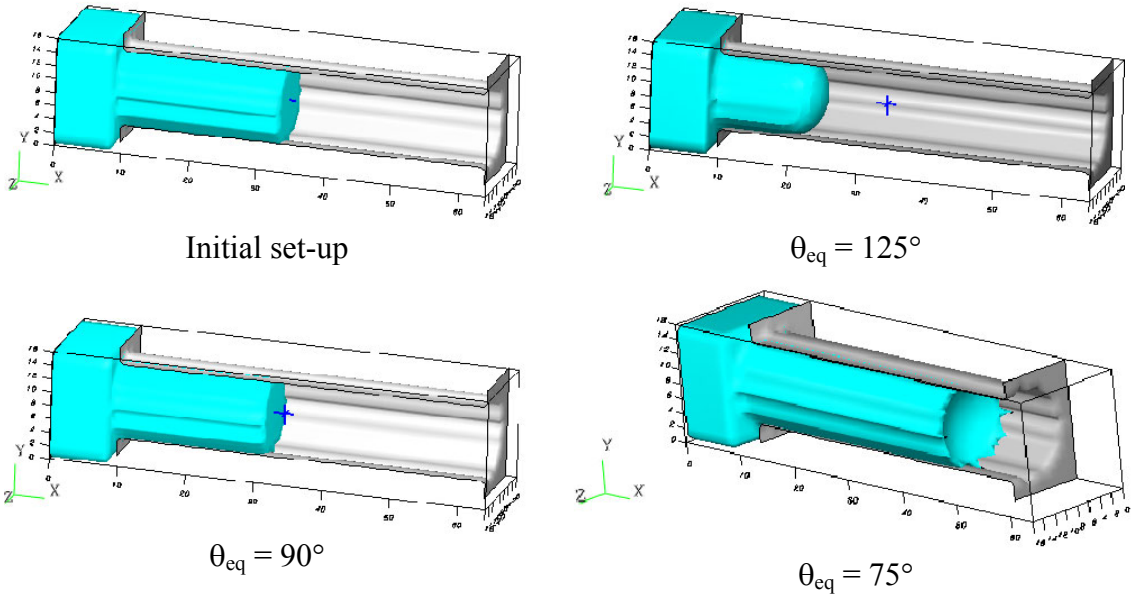

Figure 6. Liquid drainage and imbibition due to capillary action in a tube.

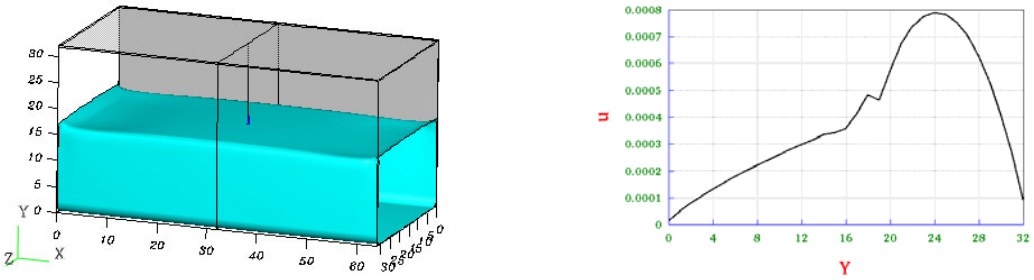

Figure 7. Separated flow of liquid and gas in a channel driven by pressure difference between inlet and outlet. The liquid to gas viscosity and density ratios are 10.

In Figure 8, we consider flow through a GDL. The computational domain is resolved with 93 nodes in the flow direction and 64×64 nodes at the plane normal to it. Unit node spacing corresponds to 3.4μm. The GDL is 200μm thick comprising of 25 layers of carbon fibers of diameter 8μm, the in-plane area is 218μm×218μm and porosity 0.78. An open space of thickness 109μm is provided at the gas-channel side to allow liquid-breakthrough and formation of multiple droplets. Liquid is introduced at the boundary on the catalyst side. The side-boundaries are no-slip walls of neutral wettability i.e. $\theta_{eq} = 90^{\circ}$. In Figure 8, snap-shots of liquid-breakthrough are shown at different fiber hydrophobicity. Liquid breaks through the channel side of the GDL in the form of droplets. These droplets may coalesce forming larger drops. As the hydrophobicity is increased the saturation at the break-through decreases. Liquid flows as small streams leading to surface pores. These observations are consistent with other published data [14-16].

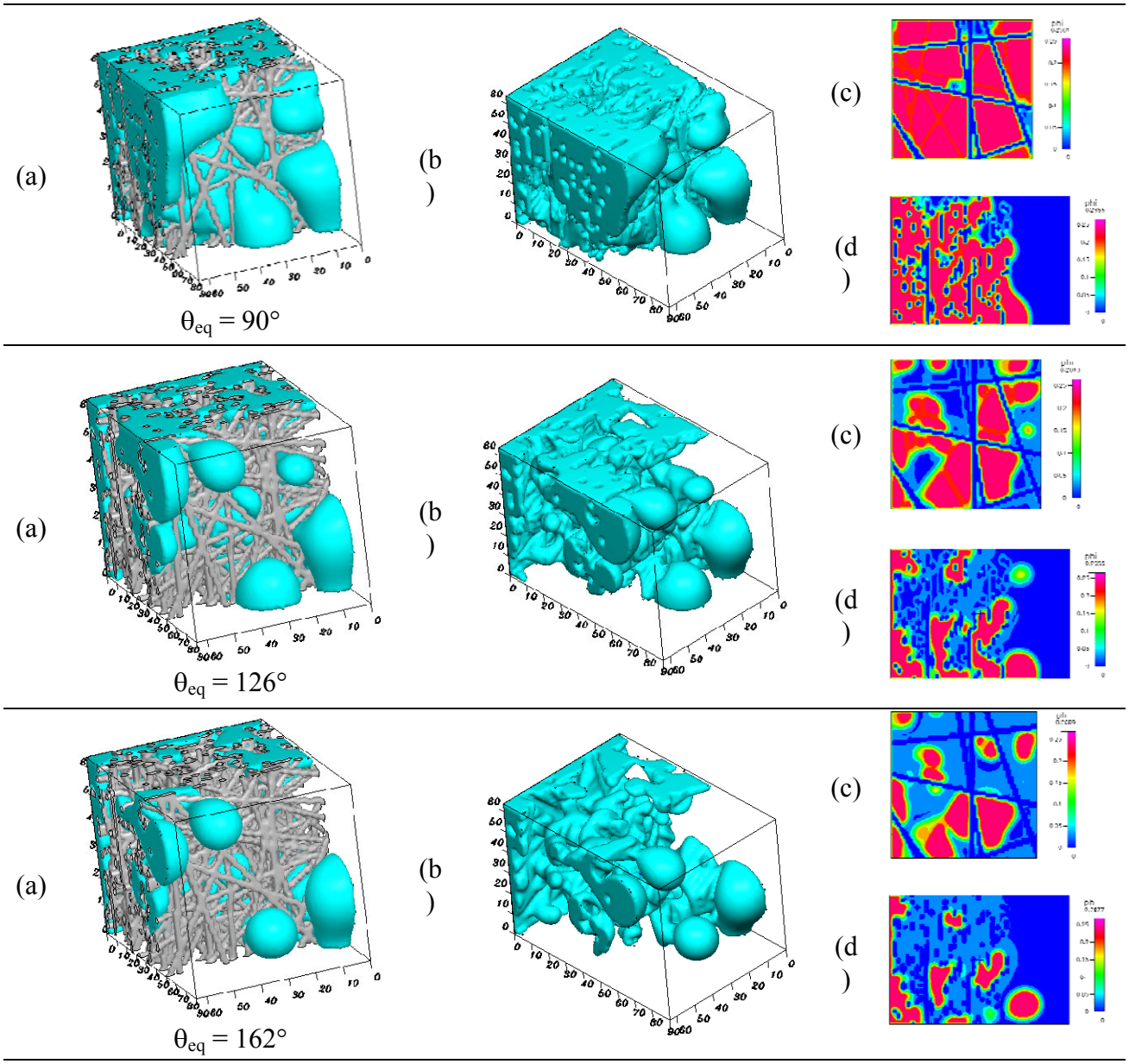

Figure 8. Influence of fiber wettability on liquid saturation as it breaks through the porous gas-diffusion layer (GDL). (a) Emergence of liquid drops at the GDL and gas-channel interface. (b) Liquid distribution inside the porous medium. (c) Liquid-gas distribution on a plane normal to the flow. (d) Liquid-gas distribution on a plane parallel to the flow. Liquid saturation decreases as fiber hydrophobicity increases.

Conclusions

In this work, the lattice-Boltzmann method (LBM) is demonstrated as an effective numerical tool in modeling single and multiphase transport through porous microstructures representing the gas-diffusion-layer of a PEM Fuel Cell. The model is suitable to capture effects of fiber orientation, external compression, and capillary pressure for multiphase transport. Flows through carbon paper

GDL show emergence of liquid droplets from the gas-channel side. The fiber hydrophobicity has strong influence on the liquid flow paths inside the GDL. As hydrophobicity increases liquid flows as separated streams, resulting in a low liquid saturation at break through.

Acknowledgments

This material is based upon work supported by the Department of Energy under award number DE-FG36-07G017010.

Disclaimer

References

1. He X., Chen, S. and Zhang, R. (1999), *J. Comp. Phys.*, 152, 642.
2. Mukherjee S. and Abraham, J. (2007), *J. Coll. Inter. Sci.*, 312, 341.
3. Mukherjee S. and Abraham, J. (2007), *Phys. Fluids*, 19, 052103.
4. Mukherjee,S., Cole, J.V., Jain, K., and Gidwani, A. (2008), 214th Meeting of Electrochemical Society, Honolulu, HI, Oct. 12-17.
5. Schulz, V. P., Becker, J., Wiegmann, A., Mukherjee, P.P., and Wang, C.Y. (2007), *J. Electrochem. Soc.,* 154, B419.
6. Niu, X. D., Munekata, T., Hyodo, S.A. and Suga, K. (2007), *J. Power Sources*, 172, 542.
7. Mukherjee S. and Abraham, J. (2007), *Phys. Rev. E*, 75, 026701.
8. Mukherjee S. and Abraham, J. (2007), *Computers Fluids*, 36, 1149.
9. Bhatnagar, P., Gross, E. and Krook, M. (1954), *Phys. Rev.*, 94, 511.
10. D'Humie′res, D., Ginzburg, I., Krafczyk, M., Lallemand, P., and Luo, L.S. (2002) *Phil. Trans. Roy. Soc. Lon. A*, 360, 437.
11. Yiotis, A.G., Psihogios, J., Kainourgiakis, M. E., Papaioannou, A., and Stubos, A.K. (2007), *Coll. Surf. A: Physiochem. Eng. Aspects*, 300, 35.
12. Martys, N.S. and Hagedorn, J.G. (2002), *Materials and Structures*, 35, 650.
13. Dohle, H., Jung, R., Kimiaie, N., Mergel, J., and Müller, M. (2003), *J. Power Sources*, 124**,** 371.
14. Lister, S., Sinton, D. and Djilali, N. (2006), *Journal of Power Sources*, 154, 95-105.
15. Bazylak, A., Sinton, D., Liu, Z.-S., and Djilali, N. (2007), *Journal of Power Sources*, 163, 784-792.
16. Bazylak, A., Sinton, D., and Djilali, N. (2008), *Journal of Power Sources*, 176, 240-246.